View Article Online / Journal Homepage / Table of Contents for this issue
Dynamic Article Links

Analyst

Cite this: *Analyst*, 2011, **136**, 4507

www.rsc.org/analyst

PAPER

Single on-chip gold nanowires for electrochemical biosensing of glucose†

Karen Dawson, Marine Baudequin and Alan O'Riordan*

Received 4th April 2011, Accepted 23rd August 2011
DOI: 10.1039/c1an15279c

The development of glucose diagnostic devices with low detection limits is of key importance in diabetes-related research. New highly sensitive sensors are required for non-invasive detection of glucose in bodily fluids, other than blood, and an electrochemical sensor based on a single gold nanowire for rapid, reliable and quantitative detection of low glucose concentrations (10 μM–1 mM), is presented in this paper. Single gold nanowire devices are fabricated at silicon chip substrates using a hybrid electron beam – photolithography approach. Critical dimensions of the nanowires are characterised using a combination of scanning electron and atomic force microscopies. Fabricated nanowire devices are characterised by direct electrical probing and cyclic voltammetry to explore functionality. The voltammetric detection of glucose was performed using ferrocene monocarboxylic acid as an oxidising mediator in the presence of glucose oxidase. The biosensor can be applied to the quantification of glucose in the range of 10 μM–100 mM, with an extremely high sensitivity of 7.2 mA mM^{-1} cm^{-2} and a low detection limit of 3 μM (S/N = 3). The sensor demonstrated high selectivity towards glucose with negligible interference from other oxidizable species including uric acid, ascorbic acid, mannose, fructose, salicylic acid (Aspirin) and acetaminophen (Paracetamol).

Published on 12 September 2011. Downloaded by Michigan State University on 22/09/2013 05:36:41.

Introduction

In recent years, the application area of biosensors has experienced substantial growth with the global biosensor market estimated to exceed $14.42 billion by 2016.[1] The emerging trend for point-of-care instrumentation is driving the development of miniaturised systems capable of reliable and rapid quantification of a wide range of biomolecules.[2–5] At present, glucose detection is of major importance due to the increasing prevalence of diabetes mellitus.[6] The dominant assay paradigm for measurement of glucose is based on a blood droplet obtained from a finger pin prick; a process which can be painful. Capillary glucose is typically in the ~4–7 mM concentration range (for healthy adults) well within the capability of commercially available devices.[7,8] However, non-invasive analysis of glucose, *i.e.*, from other bodily fluids such as saliva (~100–500 μM),[7,9] requires much lower detection limits and consequently the need to develop new generations of sensors that exhibit much higher glucose sensitivity.

One-dimensional (1D) nanostructures are attractive building blocks for future sensing devices and systems. For example, diagnostic devices that employ nanowires for direct, sensitive and rapid detection of biological and chemical species represent a new and emerging powerful class of sensors.[2,3,10–14] Noble metal nanowires such as gold, platinum and silver, are especially important because of their excellent electrical and optical properties. Nanowire sensors based on electrochemical, surface enhanced plasmon resonance and surface enhanced Raman scattering detection mechanisms have been reported.[15–18] Gold nanowires are of particular interest due to their high chemical and thermal stability, biocompatibility and excellent electrical conductivity. While a number of techniques for nanowire fabrication have been reported,[13,17,19–25] a versatile approach for fabrication of robust nanowires is Electron Beam Lithography (EBL), metal deposition and lift-off. This approach produces on-chip nanowires with well defined geometries that are easily contactable with overlaid interconnecting electrodes (using standard micron-scale photolithography techniques).

Gold nanowires have tremendous potential as new enzyme-based electrochemical biosensors exhibiting significant performance enhancements compared to micro and ultra-micro electrodes. As the critical dimensions of an electrode enters the nano regime, radial analyte diffusion to the electrode dominates, resulting in increased rates of mass transport, higher current densities, reduced parasitic capacitance, higher signal to noise ratios, lower detection limits and steady-state voltammograms at high measurement rates.[26] Nanowire electrodes fabricated at silicon chip substrates permit interfacing with electronic circuitry that can allow assay multiplexing with real-time signal readout, the possibility of rapid data processing and also the possibility of employing microfluidic-based sample delivery approaches. Although biosensing at gold nanowires ensembles has been demonstrated, surprisingly, to the best of our knowledge, the use of single on-chip gold nanowires for biosensing applications has

Nanotechnology Group, Tyndall National Institute – University College Cork, Lee Maltings, Cork, Ireland. E-mail: alan.oriordan@tyndall.ie
† Electronic supplementary information (ESI) available. See DOI: 10.1039/c1an15279c

Published on 12 September 2011. Downloaded by Michigan State University on 22/09/2013 05:36:41.

not been reported.[19,27,28] In this work, we explore the application of single on-chip gold nanowires for use as electrochemical biosensors employing glucose as a key target biomolecule. A redox mediator, ferrocene monocarboxylic acid (FcCOOH) was employed to overcome issues associated with oxygen consumption and to reduce the overpotential thereby eliminating interference effects, while also amplifying the electrochemical signal.[29] The nanowire-based devices demonstrated rapid glucose detection across the linear concentration range of 10 μM to 1 mM with a theoretical limit of detection of 3 μM (S/N = 3) and exhibited excellent selectivity to glucose in the presence of a variety of common interferent species.

Experimental

Nanowire fabrication

Nanowire electrodes were fabricated using a hybrid electron beam-photolithography process on four inch wafer silicon substrates bearing a ~300 nm layer of thermally grown silicon dioxide. In this approach, nanowire and alignment marks were written by direct write electron beam lithography (JBX-6000FS, JEOL UK Ltd., optimised parameters: beam voltage 50k V, beam current 100 pA and beam dose 120 μC cm^{-2}) in resist (ZEP 520 Nippon Zeon). Following resist development, Ti/Pt/Au (5/5/30 nm) layers were blanket deposited by evaporation (Temescal FC-2000 E-beam evaporator) and removed from un-patterned areas using standard lift-off techniques to yield stacked metallic (Ti/Pt/Au) nanowire structures. Using the E-beam written alignment marks for alignment and registration, interconnection tracks were then overlaid onto nanowire termini using photolithography, metal deposition (Ti/Au 10/200 nm) and lift-off. Each chip contained seven individually contacted nanowires separated by a gap of 1.5 μm to allow inter- and intra-chip variation analysis. A thick layer of photoresist (Shipley S1813, ~1 μm) was then spin coated onto the wafer surface and photolithography employed to open a window (~40 μm × 50 μm) in the photoresist directly over the nanowires. This process was optimised such that the interconnection remained covered by the insulating photoresist layer thereby ensuring direct contact only between the nanowires and the external electrolyte solution. Finally, to complete device packaging, chips were assembled onto specifically designed printed circuit boards, electrically contacted using wedge wire bonding (25 μm gold wires) and the bond wires protected using epoxy.

Nanowire characterisation

Optical micrographs were acquired using a calibrated microscope (Axioskop II, Carl Zeiss Ltd.) equipped with a charge-coupled detector camera (CCD; DEI-750, Optronics). Scanning electron microscopy (SEM) images of single Au nanowires were acquired using a field emission SEM (JSM-6700F, JEOL UK Ltd.) operating at beam voltages between 5 and 10 kV. The topography of individual nanowires was characterised using a calibrated atomic force microscope (AFM; Dimension 3100, Veeco Instruments Inc.) in tapping mode with commercial tapping mode probes (MP-11100, Veeco Instruments Inc; typical radius of curvature ~ 10 nm and front/side cone angles of 15°/17.5°, respectively). Two-point electrical measurements were performed using a probe station (Model 6200, Micromanipulator Probe Station) in combination with a source meter (Keithly 2400) programmed using LabVIEW™. For these current–voltage (*I–V*) measurements, the source electrode was grounded, a bias sweep up to ± 10 mV was applied to the drain electrode, and the current through the nanowire was measured.

Electrochemical analysis

All electrochemical studies were performed using a CHI660a Electrochemical Analyzer and Faraday Cage CHI200b (CH Instruments). A three-electrode cell was adopted, employing a single nanowire electrode as working electrode, with platinum coil (BAS Inc.) as the counter electrode and a saturated Ag/AgCl reference electrode (CH Instruments). A detailed description and schematic of the cell setup are provided in the supporting information. Cyclic voltammetry measurements were carried out in the potential range 0.0 to 0.6 V at a range of scan rates (5, 10, 20, 50 and 100 mVs^{-1}). Unless otherwise stated, all chemicals were obtained from Sigma Aldrich. Enzymatic mediated detection of glucose was performed employing 10 mM ferrocenemonocarboxylic acid, (FcCOOH, Alfa Aesar) in 10 mM phosphate buffered saline (PBS) pH 7.4 with 1 mg ml^{-1} added glucose oxidase, (GOx, *Aspergillius niger*). Glucose stock solutions were prepared using D-(+)-glucose in 10 mM, PBS. Predetermined aliquots were added sequentially to FcCOOH and GOx in PBS and agitated until homogenous. Interfering species analysis was conducted by spiking of 1 mM glucose solution, containing 1 mg ml^{-1} GOx, 10 mM FcCOOH in 10 mM PBS, with selected interferents at typical physiological concentrations. Stock solutions of uric acid (UA), L-ascorbic acid (AA), salicylic acid (Aspirin), acetaminophen (Paracetamol), D-(-)-fructose and D-(+)-mannose were prepared in 10 mM PBS All solutions were prepared daily using deionised water; 18.2 MΩ cm (ELGA Pure Lab Ultra).

Results and discussion

Nanowire characterisation

Nanowires were fabricated using a hybrid EBL and photolithography process at silicon wafer substrates bearing a 300 nm layer of thermally grown silicon dioxide, see experimental section. Each chip contained seven electrically isolated nanowire electrodes, separated by a distance of 1.5 μm, to allow for direct on chip electrical and electrochemical comparison. While it is possible to electrically short all nanowires together in order to form a nanowire array electrode, single nanowire electrode analysis was undertaken in this work. Since the enhanced mass transport of an analyte to a nanoelectrode arises from radial diffusion profiles, in an array, diffusion profiles may overlap as electrodes become closer to each other (typically ~20 times nanowire width) resulting in lower than expected current response and reduced signal to noise ratios.[26] To ensure our wires remained diffusionally independent (thereby maximising signal/noise) we performed all of our analysis at single nanowire electrodes.

Following fabrication, nanowire devices were characterized using a combination of optical microscopy, SEM and AFM. Fig. 1a shows an optical micrograph of a fully

 This journal is © The Royal Society of Chemistry 2011

Published on 12 September 2011. Downloaded by Michigan State University on 22/09/2013 05:36:41.

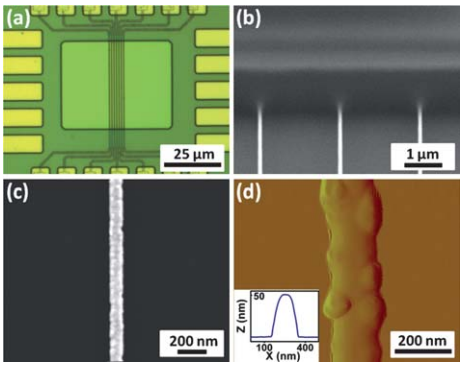

Fig. 1 (a) An optical micrograph of a fully fabricated array of individual nanowire electrode devices with interconnection tracks and an insulating photoresist overlayer. A window (40 × 50 μm, centre) was selectively opened in photoresist above the array of nanowires to permit contact with an electrolyte solution. Scale bar, 25 μm. (b) SEM micrograph of a region of the exposed array of nanowires. A portion of the remaining photoresist overlayer is shown present at top of image. Scale bar, 1 μm. (c) SEM micrograph of a single nanowire electrode, average width 100 ± 6 nm. (d) AFM micrograph of a single nanowire. Inset shows height measurement 50.6 ± 0.08 nm.

packaged array of individual nanowire devices, electrically contacted, passivated with an overlaying insulating photoresist layer. The purpose of this insulating overlayer was to prevent unwanted electrochemical reactions occurring between metal interconnection tracks and electrochemically active species. To allow direct contact only between a nanowire and electrolytic solution, a window (40 μm × 50 μm) was selectively opened in the photoresist layer, directly above the array. Post fabrication SEM characterisation clearly showed that the photoresist layer was fully removed from the entire target window region thereby exposing the underlying nanowire electrodes, see Fig. 1b.

Fig. 1c shows a typical SEM image of an individual nanowire. Statistical analysis of nanowire widths (measured at multiple locations at 18 different nanowires on 5 separate chips) showed that fabrication process was very reproducible with nanowire widths of 100 ± 6 nm being routinely achieved. Similarly, an AFM analysis undertaken, following selective removal of the insulating overlayer, indicated that no residual photoresist remained at or about the nanowires and that nanowires had a 3D profile standing proud of the silicon surface, see Fig. 1d. Statistical analysis of AFM data acquired from a number of nanowire measurements (captured from multiple locations on 5 different nanowires on 3 separate chips) showed an average height of 50.6 ± 0.8 nm, see Fig. 1d: inset. A full statistical analysis of nanowire critical dimensions is presented in the supporting information section; see Fig. S1. Nanowire length was defined by the width of the passivation window opening ~ 40 μm. This yielded a calculated nanowire geometric active surface area of 8 x10^{-8} cm^2 available for electrochemical analysis.

To confirm the functionality of packaged nanowire devices, electrical characterisation using standard two-point *I–V* measurements was performed in the voltage range of −10 mV to +10 mV. This low voltage range, was employed in order to prevent potential damage occurring to a nanowire from electromigration effects and to confirm Ohmic behaviour. Ten nanowires were characterised in this manner and each displayed linear responses confirming electrical contact to the nanowires by the interconnection tracks. Packaged nanowire devices exhibited low resistance (890–911 Ω); see Fig. 2a. Standard open- and short-circuit control experiments were also performed on the packaged chips to confirm the observed electrical characteristics were exclusively due to nanowire electrodes.

Electrochemical characterization

To undertake electrochemical experiments, a potentiostat with a Faraday cage was employed to apply an appropriate potential scan range to a nanowire working electrode with respect to a Ag/AgCl (saturated KCl) reference with Pt coil as a counter electrode. Nanoelectrodes were first electrochemically cleaned by potentiodynamic cycling in 0.1 M sulphuric acid. Cyclic voltammograms (CVs) exhibited characteristic gold and platinum oxide formation (*ca.* 1.3 V), gold reduction (*ca.* 0.78 V) and platinum reduction (*ca.* 0.26 V) peaks, respectively, see Fig. 2b.[30,31] Platinum peaks arose from the presence of platinum

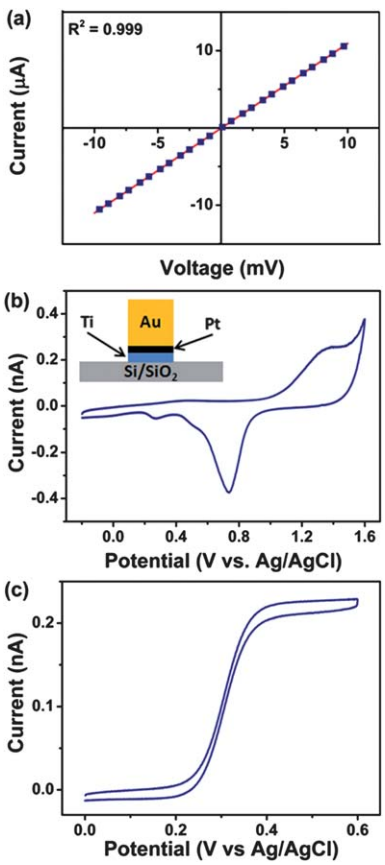

Fig. 2 (a) Two-point *I–V* characteristic measured for a typical fully integrated nanowire exhibiting Ohmic behaviour, 890–911 Ω. (b) CV obtained from a typical single gold nanowire device in 0.1 M H_2SO_4, from −0.2 to +1.6 V at 100 mV s^{-1}. The CV exhibits characteristic gold and platinum oxide formation (*ca.* 1.3 V), gold reduction (*ca.* 0.78 V) and platinum reduction (*ca.* 0.26 V) peaks. Inset: Schematic of the cross-section of a nanowire electrode. (c) Typical CV measured at a single nanowire electrode in 1 mM FcCOOH, in 10 mM PBS at 100 mV s^{-1}.

Published on 12 September 2011. Downloaded by Michigan State University on 22/09/2013 05:36:41.

in the nanowire stack; Fig. 2b inset. The magnitude of the gold reduction peak current was typically on the order of 0.2–0.4 nA. These low measured Faradic currents may be attributed to the electrochemical oxidation and reduction of gold oxide at a nanowire electrode surface and strongly suggests that the interconnection tracks were sufficiently insulated from the electrolytic solution by the resist overlayer.

With regard to nanowire electrode reproducibility, we performed voltammetry experiments in 1 mM FcCOOH, at 100 mV s^{-1} for a variety of different nanowire electrodes; see Fig. 2c. A variation of ± 13 pA, corresponding to ~5%, in the steady-state current was measured (~ 225 pA) at individual nanowire electrodes on the same chip (intra-chip) and at nanowires on different chips (inter-chip) was determined experimentally. We believe that this variation across these nanowires may be accounted for by differences in the exact nanowire electrode surface area arising from gold clustering and rough nanowire edges created during the metal evaporation and lift-off processes.[32] A narrow range of cell resistances arising from slight variation in separation distance between the working, reference and counter electrodes may also have contributed to this variation, although this effect would not be expected to dominate.

Glucose detection

Concerning biosensor development, gold nanoelectrodes have been used for the detection of glucose and the fabrication of oxidase-based biosensors which employ molecular oxygen as an oxidising agent.[19,27] The overall oxidation reaction of glucose is given by eqn (1). Using this approach, glucose concentration can be determined by measuring either the consumption of oxygen or the formation of gluconic acid or H_2O_2.

$$\text{Glucose} + O_2 \xrightarrow{\text{GOx}} \text{gluconic acid} + H_2O_2 \quad (1)$$

Although these devices work quite well they suffer from a number of key limitations as follows: The ambient concentration of dissolved oxygen needs to be controlled and constant – otherwise the electrode response to the decrease of in oxygen concentration would not be proportional to the decrease in glucose concentration. Relatively high reduction and oxidising potentials are required to reduce oxygen (*ca.* −0.7 V *versus* SHE) or oxidise enzymatic product H_2O_2 (*ca.* 0.65 V *versus* SHE) which are sufficient to reduce or oxidise common interferents normally present in biological fluids.,[27,33,34] To address these limitations, research has focused on replacing oxygen with other oxidising agents 'mediators' based on transition metal cations and their complexes whose concentrations may be controlled.[23] Mediators typically have fast electron transfer kinetics, react rapidly with the enzyme, have a low overpotential for regeneration and are stable in both their oxidised and reduced forms.

To explore the potential of single on-chip gold nanowires for use as a glucose sensor we employed FcCOOH as an oxidising mediator. FcCOOH was selected due to its relatively high solubility in aqueous solutions and high diffusion coefficient ~ 5 × 10^{-6} cm^2 s^{-1}.[31] The operation of the sensor system is shown schematically in Fig. 3a. The oxidation of a glucose molecule is performed by the flavin-adenine dinucleotide (FAD) component

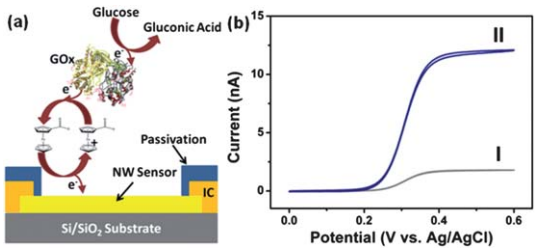

Fig. 3 (a) A schematic representation of the reaction mechanism for FcCOOH mediated electrochemical detection of glucose *via* oxidation by dissolved glucose oxidase at a gold nanowire electrode. (b) Cyclic voltammograms at a single nanowire electrode of 60 mM glucose in 10 mM FcCOOH and in 10 mM PBS in the absence (grey line) and presence (navy line) of 1 mg ml^{-1} GOx at 10 mV s^{-1}. A ~7 fold increase in limiting current is observed upon the addition of GOx.

of the glucose oxidase enzyme. In the oxidation process, FAD is reduced to $FADH_2$ (GOx_{red}) as shown in eqn (2). The $FADH_2$ is then re-oxidised to FAD by $FcCOOH^+$ which is in turn reduced to FcCOOH (3). Finally, FcCOOH is re-oxidised to $FcCOOH^+$ at the nanowire electrode given by eqn (4).[8,34,35] This final step produces a measureable current which is directly proportional to the glucose concentration as the oxidised form of the mediator is regenerated.

$$\text{Glucos} + GOx_{ox} \rightarrow \text{Gluconic acid} + GOx_{red} + 2H^+ \quad (2)$$

$$GOx_{red} + 2FcCOOH_{ox} \rightarrow GOx_{ox} + 2FcCOOH \quad (3)$$

$$2FcCOOH - 2e^- \rightarrow 2FcCOOH_{ox} \quad (4)$$

To highlight this process, curve I in Fig. 3b shows a typical CV acquired in the voltage range of 0.0–0.6 V using a gold nanowire device in 60 mM glucose solution, 10 mM FcCOOH in 10 mM PBS, pH 7.4 and 25 °C, at 10 mVs^{-1}. CVs display the typical steady-state behaviour observed at nanoelectrodes for the single-electron oxidation of FcCOOH.[26] Due to the small critical dimensions of the nanowires, mass transport to a nanowire is highly effective and becomes comparable to or larger than the rate of electron transfer from the FcCOOH to the electrode surface as has been previously shown using gold nanowire electrodes.[18] The optimisation of electrolyte composition is presented in the supporting information; see Fig S3.

To confirm that this high mediator concentration did not result in a saturated signal at the nanowire electrodes, we calculated the theoretical limiting current expected for a single nanowire using the nanoband eqn (5): [36]

$$i_L = \frac{2n\pi FCDl}{\ln(64\,Dt/w^2)} \quad (5)$$

where n is the number of electrons transferred, F is Faraday's constant, C is the concentration of the mediating species, D is the diffusion coefficient of the mediator, l is the length of the band electrode and t is the time (equal to RT/Fv, where R is the gas constant, T is temperature, v is the scan rate) and w is nanowire width. The determined value of 1.910 nA is in excellent agreement with that experimentally measured, 1.869 ± 0.001 nA,

 This journal is © The Royal Society of Chemistry 2011

Published on 12 September 2011. Downloaded by Michigan State University on 22/09/2013 05:36:41.

indicating that this high mediator concentration is commensurate with this glucose detection approach.

On addition of 1 mg ml^{-1} GOx, a significant increase in steady-state current (~ 7 fold) was observed, see curve II in Fig. 3b. This current amplification arises from the regeneration of FcCOOH from the $FcCOOH^+$ ion by the enzyme in its reduced form. No Faradic currents were observed within the potential range of 0.0–0.6 V during control experiments performed using glucose only in PBS solution or GOx in PBS solution. These results strongly indicate that nanowire electrodes were compatible with glucose detection in PBS buffer solutions. Furthermore the high steady-state Faradic currents shown in Fig. 3b indicated that nanowire electrodes could facilitate glucose detection at low glucose concentrations.

To undertake experiments, predetermined aliquots of glucose were added sequentially to 10 mM FcCOOH and 1mg ml^{-1} GOx in 10 mM PBS and agitated until homogenous. Fig. 4a shows CVs obtained for the bio-electrocatalytic oxidation of glucose in the concentration range of 10 μM–1 mM (typical saliva direct concentrations). Data are expressed in current density to allow back comparison with the literature and also to determine sensitivity of glucose detection. CVs exhibited steady-state behaviour for all concentrations at pH 7.4, and scan rate 10 mV s^{-1}. An increase in measured Faradic current with increasing glucose concentration was observed. Experiments were repeated in triplicate and exhibited excellent reproducibility with an average error of 5 pA, corresponding to 0.25%, measured across all data points for all concentrations. This high reproducibility is reflected in the calibration plots included in Fig. 4 (b and d), where the very narrow error bars can be seen within the data points. Individual nanowires exhibited a linear electro-oxidative response towards glucose (data points obtained from CVs at 0.6 V). Fig. 4b displays the calibration plot for glucose between 10 μM–1 mM with a linearity of $R^2 = 0.993$ and a sensitivity of 7.2 mA mM^{-1} cm^{-2}. This enhanced sensitivity arises from increased radial diffusion of the analyte in the nano-regime, resulting in increased mass transport to a nanowire electrode allowing for rapid analysis of glucose at lower background electrolyte concentrations, lower interfacial capacitance and higher achievable current densities. From the deviation in the baseline, a theoretical limit of detection of 3 ± 0.1 μM (S/N = 3) was determined. This is a reasonable detection limit since aliquots of 10 μM produced well resolved CVs with a good signal to noise ratio.

Concerning a higher glucose concentration range corresponding to capillary glucose levels, typical CVs of glucose bio-electrocatalytic oxidation in the 1–100 mM concentration regime are presented in Fig. 4c. CVs exhibited steady-state behaviour and an increase in measured Faradic current for increasing glucose concentration was also observed. Fig. 4d displays the calibration plot for glucose between 1 mM–100 mM with a linearity of $R^2 = 0.995$, a sensitivity of 1.8 mA mM^{-1} cm^{-2} and a lower limit of detection of 16 μM (S/N = 3) was determined. The reduced sensitivity in voltammetric response at these higher

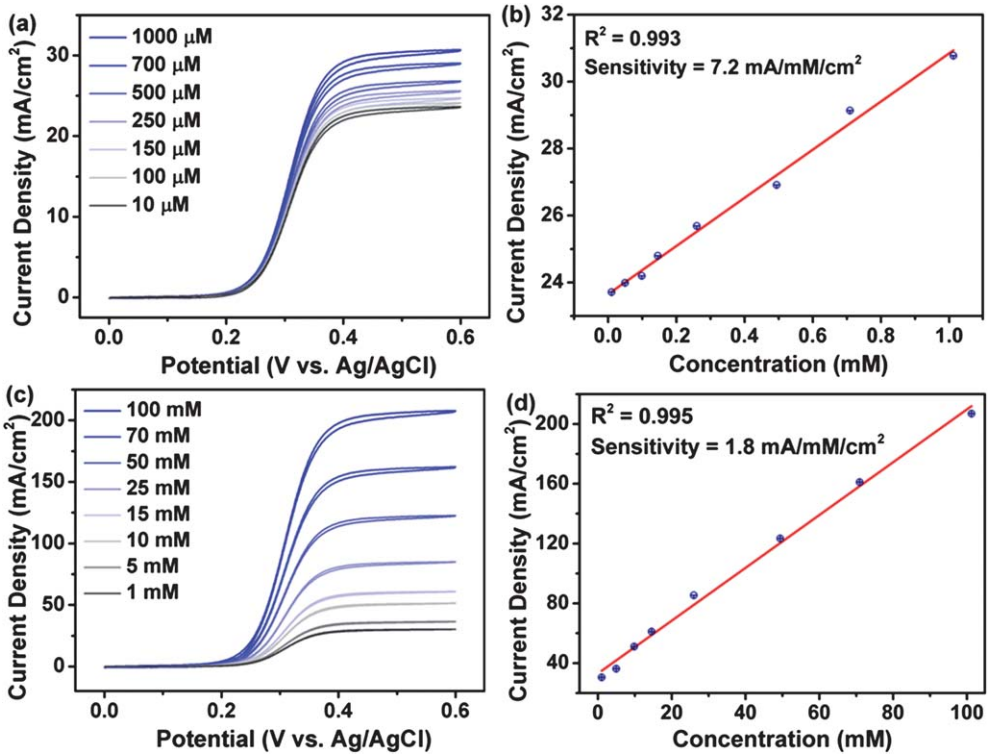

Fig. 4 (a) Steady-state CVs measured at a single nanowire in 10 mM FcCOOH and 1 mg ml^{-1} GOx in 10 mM PBS with increasing concentrations of Glucose (10 μM to 1 mM). (b) Background subtracted calibration plot of average steady-state current observed at 0.6 V *versus* concentration of glucose 10 μM to 1 mM. (c) Steady-state CVs measured for increasing concentrations of glucose (1 mM to 100 mM). (d) Background subtracted calibration plot of average steady-state current observed at 0.6 V *versus* concentration of glucose 1 mM to 100 mM. All CVs were recorded at 10 mV s^{-1}. Error bars are included in the calibration plots.

Published on 12 September 2011. Downloaded by Michigan State University on 22/09/2013 05:36:41.

glucose concentrations may arise from the active FAD sites of the glucose oxidase enzyme becoming saturated.[27]

Interfering species

The effects of substances which might interfere with the response of the nanowire electrodes, either through direct electrode oxidation, reaction with mediator or direct enzymatic interactions were explored. Analyses of buffered solutions containing 1 mM glucose (in 1 mg ml^{-1} GOx, 10 mM FcCOOH), with added oxidizable interferents (higher than normal physiological concentrations) and other sugars (at their physiological concentrations) were undertaken.[27,33] CVs were carried out in the potential range 0.0 to 0.6 V, scan rate 50 mV s^{-1}. The steady-state current signal obtained for a 1 mM glucose solution, I_0, was normalised to 100%. The measured current for each interferent species, I, in the presence of 1 mM glucose is expressed as a percentage of glucose ($I/I_0 \times 100$) for clarity. The results displayed in Table 1 demonstrate almost negligible interferences from 0.2 mM uric acid, 0.5 mM ascorbic acid, 0.5 mM salicylic acid, 0.5 mM acetaminophen, 1 mM fructose and 1 mM mannose spiked in 1 mM glucose solutions. In this manner, nanowire based electrodes demonstrate high sensitivity and selectivity to glucose detection against common interferent species that normally co-exist with glucose in biological matrices.

Electrode stability

We undertook multiple measurements over a period of months and nanowires were observed to be stable under reasonable experimental conditions. Over the course of our experiments we did not observe electrode fouling during glucose detection with or without presence of interferents under normal physiological concentrations. Between analyses we undertook repeated potentiodynamic cycling (0–1.3 V) in sulphuric acid (0.1 M) as an electrochemical cleaning step. Typically 10–14 cycles were sufficient to clean the nanowires. Cleaning was determined to be complete when the magnitude and shape of the gold oxide reduction peak current (ca 0.78 V) was observed to remain constant. However, continuous and excessive cycling (>200 cycles) was observed to seriously degrade wire quality eventually leading to a break in the nanowire and formation of open circuits.

Table 1 Table of Interfering Species

Interfering Species	Interferent concentration	$(I/I_0 \times 100)^a$
Ascorbic Acid	0.5 mM	98.38%
Uric Acid	0.2 mM	101.17%
Salicylic Acid	0.5 mM	99.11%
Acetaminophen	0.5 mM	98.89%
Fructose	1 mM	100.21%
Mannose	1 mM	97.41%

[a] Where I_0 is the signal response obtained from 1.0 mM glucose in 10 mM PBS.

Conclusion

Individual gold nanowires, with highly reproducible critical dimensions, were fabricated a hybrid EBL-photolithography process on silicon substrates. Mediated enzymatic detection of the key target analyte glucose was demonstrated at individual nanowire devices. The steady-state voltammetric response was linear across the voltage range of 10 μM to 1 mM with a sensitivity of 7.2 mA cm^{-2} mM^{-1}, with a theoretical detection limit of 3 μM (S/N = 3). Measurements undertaken in the presence of common interfering species exhibited negligible signal contributions suggesting high selectivity for glucose. The wide dynamic range, high sensitivity and selectivity coupled with good the biocompatibility of the gold nanowire electrode opens up the possibility of employing nanowire electrodes as sensors in future non-invasive glucose diagnostic devices employing, for example, saliva which typically has glucose present in ~100–500 μM range. Although we employed both GOx and FcCOOH free in solution in this work, ongoing research is now focusing on the immobilisation of both mediator and enzymes for a range of important biomolecules at gold nanowire electrode surfaces coupled with the development of microfluidics for sample delivery.

Acknowledgements

This work was supported by Science Foundation Ireland under the Research Frontiers Programme (SFI/09/RFP/CAP2455) by the European Commission under the FP7 ICT project "E-Brains" (257488), and FP7 ICT project "Nanofunction" (257375).

References

1 Frost and Sullivan, *Analytical Review of World Biosensors Market*, 2007.
2 J. Hahm and C. M. Lieber, *Nano Lett.*, 2004, **4**, 51–54.
3 X. Wang and C. S. Ozkan, *Nano Lett.*, 2008, **8**, 398–404.
4 C. O. Parker, Y. H. Lanyon, M. Manning, D. W. M. Arrigan and I. E. Tothill, *Anal. Chem.*, 2009, **81**, 5291–5298.
5 M. Manning and G. Redmond, *Langmuir*, 2005, **21**, 395–402.
6 S. P. Chen, J. A. Wu, X. D. Yu, J. J. Xu and H. Y. Chen, *Electrophoresis*, 2010, **31**, 3097–3106.
7 M. S. M. Soares, M. M. V. Batista, M. J. Pimentel, I. L. A. Passos and E. Chimenos-Kustner, *Medicina Oral Patología Oral y Cirugia Bucal*, 2009, **14**, E510–E513.
8 J. Wang, *Chem. Rev.*, 2008, **108**, 814–825.
9 M. L. Di Gioia, A. Leggio, A. Le Pera, A. Liguori, A. Napoli, C. Siciliano and G. Sindona, *J. Chromatogr., B: Anal. Technol. Biomed. Life Sci.*, 2004, **801**, 355–358.
10 K. Ramanathan, M. A. Bangar, M. Yun, W. Chen, N. V. Myung and A. Mulchandani, *J. Am. Chem. Soc.*, 2005, **127**, 496–497.
11 M. A. Bangar, C. M. Hangarter, B. Yoo, Y. Rheem, W. Chen, A. Mulchandani and N. V. Myung, *Electroanalysis*, 2009, **21**, 61–67.
12 R. H. Wang, C. M. Ruan, D. Kanayeva, K. Lassiter and Y. B. Li, *Nano Lett.*, 2008, **8**, 2625–2631.
13 K. Dawson, J. Strutwolf, G. Herzog, D. W. M. Arrigan, A. J. Quinn and A. O'Riordan, *ECS Transactions*, 2010, **28**.
14 M. Garcia and A. Escarpa, *Biosens. Bioelectron.*, 2011, **26**, 2527–2533.
15 M. Moskovits, *Rev. Mod. Phys.*, 1985, **57**, 783.
16 T. Neumann, M. L. Johansson, D. Kambhampati and W. Knoll, *Adv. Funct. Mater.*, 2002, **12**, 575–586.
17 X. Y. Zhang, D. Li, L. Bourgeois, H. T. Wang and P. A. Webley, *ChemPhysChem*, 2009, **10**, 436–441.
18 K. Dawson, J. Strutwolf, K. P. Rodgers, G. Herzog, D. W. M. Arrigan, A. J. Quinn and A. O'Riordan, *Anal. Chem.*, 2011, **83**, 5535–5540.

 This journal is © The Royal Society of Chemistry 2011

View Article Online

19 X. Zhang, D. Li, L. Bourgeois, H. Wang and P. A. Webley, *ChemPhysChem*, 2009, **10**, 436–441.
20 S. Keebaugh, A. K. Kalkan, W. J. Nam and S. J. Fonash, *Electrochem. Solid-State Lett.*, 2006, **9**, H88–H91.
21 E. J. Menke, M. A. Thompson, C. Xiang, L. C. Yang and R. M. Penner, *Nat. Mater.*, 2006, **5**, 914–919.
22 R. Ji, W. Lee, R. Scholz, U. Gosele and K. Nielsch, *Adv. Mater.*, 2006, **18**, 2593.
23 J. Jorritsma, M. A. M. Gijs, J. M. Kerkhof and J. G. H. Stienen, *Nanotechnology*, 1996, **7**, 263–265.
24 E. C. Walter, B. J. Murray, F. Favier, G. Kaltenpoth, M. Grunze and R. M. Penner, *J. Phys. Chem. B*, 2002, **106**, 11407–11411.
25 J. Chai, D. Wang, X. N. Fan and J. M. Buriak, *Nat. Nanotechnol.*, 2007, **2**, 500–506.
26 D. W. M. Arrigan, *Analyst*, 2004, **129**, 1157–1165.
27 M. Delvaux, S. Demoustier-Champagne and A. Walcarius, *Electroanalysis*, 2004, **16**, 190–198.
28 J. Jimenez, R. Sheparovych, M. Pita, A. Narvaez Garcia, E. Dominguez, S. Minko and E. Katz, *J. Phys. Chem. C*, 2008, **112**, 7337–7344.
29 A. Chaubey and B. D. Malhotra, *Biosens. Bioelectron.*, 2002, **17**, 441–456.
30 A. J. Bard, ed., *Electranlaytical Chemistry*, Marcel Dekker, INC., New York, 1976.
31 Y. H. Lanyon, G. De Marzi, Y. E. Watson, A. J. Quinn, J. P. Gleeson, G. Redmond and D. W. M. Arrigan, *Anal. Chem.*, 2007, **79**, 3048–3055.
32 G. D. Marzi, D. Iacopino, A. J. Quinn and G. Redmond, *J. Appl. Phys.*, 2004, **96**, 3458–3462.
33 Z. J. Zhuang, X. D. Su, H. Y. Yuan, Q. Sun, D. Xiao and M. M. F. Choi, *Analyst*, 2008, **133**, 126–132.

Published on 12 September 2011. Downloaded by Michigan State University on 22/09/2013 05:36:41.